Examining Mechanisms of Variability within the Pacific Storm Track: Upstream Seeding and Jet-Core Strength

SANDRA M. PENNY AND DAVID S. BATTISTI

Department of Atmospheric Sciences, University of Washington, Seattle, Washington

GERARD H. ROE

Department of Earth and Space Sciences, University of Washington, Seattle, Washington

(Manuscript received 31 December 2011, in final form 19 October 2012)

ABSTRACT

This paper examines how variations in two mechanisms, upstream seeding and jet-core strength, relate to storminess within the cold season (October–April) Pacific storm track. It is found that about 17% of observed storminess covaries with the strength of the upstream wave source, and the relationship is robust throughout the cold season and for both the Pacific and Atlantic basins. Further analyses of the intraseasonal variability in the strength and structure of the wintertime [December–February (DJF)] Pacific jet stream draw upon both Eulerian-variance and feature-tracking statistics to diagnose why winter months with a strong-core jet stream have weaker storminess than those with a weak-core jet stream. Contrary to expectations, it is shown that the basic spatial patterns actually conform to a simple linear picture: regions with a weaker jet have weaker storminess. The overall decrease in storminess is most strongly linked to the weaker amplitude of individual storms in strong-core months. Previously proposed mechanisms are evaluated in the context of these new results. Last, this analysis provides further evidence that the midwinter suppression in storminess over the North Pacific Ocean is primarily due to a notable lack of storminess upstream of the Pacific storm track in the heart of winter.

1. Introduction

Linear theories of baroclinic instability were first proposed shortly after the formulation of the quasi-geostrophic equations (e.g., Charney 1947; Eady 1949), and they have provided remarkable insight into the controls on midlatitude synoptic storms. These linear scaling relationships have been invoked to make predictions about the large-scale controls on climatological storminess as a function of mean climate state, both future and past, with a great deal of success (e.g., Nakamura and Shimpo 2004; Li and Battisti 2008).

However, no linear theory can be a complete description of storm-track dynamics, and a wealth of studies have investigated other aspects of midlatitude eddies (e.g., Thorncroft et al. 1993). Observations of the Pacific storm track have also called into question the applicability of linear theory. In particular there are two aspects of the North Pacific storm-track's behavior, the climatological seasonal cycle of storminess and the intraseasonal variability of storminess within the winter season, that apparently contravene linear predictions. We describe each below.

A midwinter minimum (MWM) is observed in the strength of the climatological North Pacific storm track (Nakamura 1992). The minimum occurs despite the fact that regional temperature gradients and jet stream winds are strongest in winter, which the simplest linear theories would predict leads to the largest growth rates (e.g., Lindzen and Farrell 1980), though we note linear theory can be adapted for many other basic states (e.g., Frederiksen 1978, 1979; Ioannou and Lindzen 1986; Harnik and Chang 2004; Frederiksen and Frederiksen 2007). Many possible dynamical reasons for this behavior have been proposed and investigated (e.g., Christoph et al. 1997; Zhang and Held 1999; Chang 2001; Nakamura et al. 2002; Nakamura and Sampe 2002; Yin 2002; Harnik and Chang 2004). In a recent study, Penny et al. (2010, hereafter PRB10), used feature-tracking techniques to show that the MWM occurs primarily because there is

Corresponding author address: Sandra Penny, University of Washington, 408 ATG Building, Box 351640, Seattle, WA 98195.
E-mail: smpenny@atmos.washington.edu

DOI: 10.1175/JCLI-D-12-00017.1

a midwinter reduction in storminess over Asia, upstream of the Pacific storm track (see also Park et al. 2010). As a result, fewer and smaller seed disturbances propagate into the Pacific storm track. PRB10 showed that this is, in fact, broadly consistent with linear expectations: seed disturbances from Asia are reduced in midwinter consistent with an increase in low-level static stability associated with the Siberian high, and this remote signal propagates downstream to cause the MWM. On the other hand, PRB10 also showed that while Pacific storm-track growth rates do not have a minimum in midwinter, they do not have a maximum either. Instead, growth rates stay relatively constant throughout the winter months, suggesting that there is indeed behavior that is not accounted for in a wholly linear picture.

The idea that upstream effects may be important is not new, in fact it was proposed by Nakamura (1992) as a possible explanation for the MWM. The results of PRB10 were surprising for two reasons. First, nonlinearities in the winter Pacific storm track have been well documented by others (e.g., Chang 2001; Nakamura et al. 2002; Nakamura and Sampe 2002) and were previously advocated as the cause of the MWM. Second, others who have looked did not find a clear relationship between upstream seeding and storminess within the midwinter suppression season (Zhang 1997; Chang and Guo 2011, 2012). Motivated by this result, Park et al. (2010) also found evidence that seeding is the primary cause of the MWM in their GCM simulations. As part of this study, we investigate the cause of these discrepancies.

Explorations of the relationship between upstream seeding and storm-track variability are sparse. However, a few studies do exist. Zurita-Gotor and Chang (2005) employed both theory and simple modeling experiments and found that Earth's atmosphere exists in a regime where both local effects (e.g., baroclinicity) and nonlocal effects (e.g., seeding, tropical teleconnections) contribute to the overall strength of a storm track. Orlanski (2005) performed 50-day integrations of a high-resolution numerical model for the Pacific storm track. He nudged the upstream boundary by random upper-level waves and showed a clear relationship between the storm track and its upstream wave source. Donohoe and Battisti (2009) found evidence that a reduction in seeding contributes to North Atlantic storminess in GCM simulations of the Last Glacial Maximum. PRB10 was the first study that we are aware of to document the importance of seeding in observations on climatological time scales. The primary aim of section 3 in this study is to move beyond the MWM and to further dissect the relationship between upstream seeding and downstream storminess in observations of the North Pacific and North Atlantic storm tracks throughout the cold season.

The second aspect of the winter Pacific storm track that has been argued to contravene linear behavior is its *intraseasonal* variability in the winter [December–February (DJF)] season. Previous work (Chang 2001; Nakamura et al. 2002; Nakamura and Sampe 2002) has shown that there is an inverse relationship between winter storm-track intensity and jet-core strength in this region. That is, faster-than-normal Pacific jet streams (as well as the structural differences associated with a fast jet) are accompanied by weaker-than-normal storm-track intensity. Numerous publications have evaluated how dynamical mechanisms that operate locally (i.e., within the storm track itself) may give rise to the observed intraseasonal and interannual variability. For example, studies have evaluated the extent to which variability in diabatic heating (e.g., Nakamura et al. 2002; Chang 2001) or a modification to the linear models that accounts for a narrow jet stream (Harnik and Chang 2004) can account for the observations. Others studies have evaluated the importance of nonlocal forcings, such as winter monsoonal flow (Nakamura et al. 2002) and wave trapping by a strong subtropical jet stream (Nakamura and Sampe 2002). These studies make a significant contribution to our current understanding of midlatitude storm-track dynamics, but still much remains that is poorly understood.

The inverse relationship between winter storm-track intensity and jet-core strength on intraseasonal time scales is surprising for the same reason that the MWM was surprising: the simplest linear theories predict that midlatitude storminess should maximize when the jet stream, and its associated vertical shear, is strongest. Because of this similarity, it is sometimes assumed that the physics of the climatological MWM are the same as those associated with intraseasonal variations in the wintertime Pacific storm track. However, as we will show, this assumption is not valid, and it has led to some confusion in the literature. The mechanisms giving rise to the two are different (see also Chang 2001; Nakamura et al. 2002; Harnik and Chang 2004; PRB10).

This paper is divided into two parts. We first investigate the relationship between upstream seeding and downstream storminess in the Pacific and Atlantic storm tracks on both climatological (i.e., the climatological seasonal cycle, from October through April) and intraseasonal [i.e., the variability within wintertime (DJF) months] time scales. We will show that there is a general and robust correlation with seeding for the two Northern Hemisphere storm tracks that persists despite dramatic changes in baroclinicity and bottom boundary condition. These results also expand upon the conclusions of PRB10 that the MWM occurs primarily because the upstream wave source is reduced in winter compared to fall and spring. Second, we use feature-tracking statistics to investigate why there is an inverse relationship between jet-core strength and Pacific storminess on the intraseasonal time scale in winter (i.e., variability among wintertime months). We show that while overall Pacific storminess is indeed decreased during months with strong-core jet streams, the spatial pattern actually conforms to simple linear expectations: regions with a weaker jet have weaker storminess. The biggest cause of the overall decrease in storminess is that the amplitude of individual storms is weaker in strong-core months. Last, the intraseasonal wintertime (DJF) dataset does not contain a statistically significant signal for the role of seeding. This somewhat nuanced picture of intraseasonal variability is then related to previous work on the life cycles of midlatitude cyclones.

2. Methods

In the climate literature, storm tracks are generally viewed as a geographic region of enhanced synoptic wave activity in the climatological sense. In this paper we adopt that definition and use two complementary perspectives—one based on eddy variance and the other based on feature tracking—to analyze storminess within the Pacific storm track. We focus our attention primarily on upper-level (300 hPa) geopotential height, but do also discuss results from other fields and levels where appropriate.

For eddy-variance statistics, we represent storminess as the variance of geopotential height that has been 2–10-day bandpass filtered to isolate wave activity on the time scale of synoptic storms, as is common in the climate literature (e.g., Blackmon 1976; Blackmon et al. 1977). In section 3 we compare monthly average variance in an upstream and a downstream domain. To account for the time that it takes for energy to propagate between the two domains, the data for the downstream domain have been delayed by 72 h relative to the upstream domain. For example, the January monthly average is 1–31 January for the upstream domain, and 4 January–3 February for the downstream domain.

For feature-tracking statistics, we use the algorithm created by Hodges (1994, 1995, 1999) to compile an inventory of all Northern Hemisphere disturbances in the 6-hourly 40-yr European Centre for Medium-Range Weather Forecasts (ECMWF) Re-Analysis (ERA-40) dataset (Uppala et al. 2005) from October 1958 to April 2001. As in PRB10 and Hoskins and Hodges (2002), disturbances must travel at least 1000 km and last 48 h to be included in our analysis, and the minimum threshold value (relative to the background field) for the existence of a disturbance is 3 dm. The filtering scheme we implement prior to feature tracking is deliberately quite weak. While we obviously wish to remove any time-average features (e.g., the Aleutian and Icelandic lows) we also want to retain as much synoptic-scale wave activity as possible. As in PRB10, we apply a 90-day high-pass Butterworth filter to remove the seasonal cycle, and apply a spatial filter that admits only planetary wavenumbers between 5 and 42 to isolate synoptic-scale disturbances. Geopotential height is ideal for our purposes because features have an easily identified center, central magnitude is a meaningful measure of overall intensity (unlike relative vorticity), and distinguishing between cyclonic and anticyclonic disturbances is straightforward (unlike meridional wind). PRB10 has more discussion of our filtering and tracking choices.

The feature-tracking algorithm can be used to determine the density of storm tracks, which we call "number density." This is calculated from the number of storms to pass within 100 km of a latitude and longitude grid point, and not the number of storms to pass within a grid box. We make this choice, similar to what others have done (e.g., Hoskins and Hodges 2002), because a simple count by grid box tends to overemphasize the importance of slow-moving disturbances and it is also subject to noisy results when few storms are present.

Although we mostly present results for geopotential height at 300 hPa, we have also performed similar calculations using meridional wind at levels between 250 and 500 hPa. Results from these fields are very similar, with some caveats that we discuss in the text. In addition, results found using the whole record (1958–2001) also hold for the satellite era (1979–2001). Unless otherwise stated, all confidence intervals are determined from a Student's t test, and 95% confidence is required for statistical significance. We reserve the word "significant" to mean that a test for statistical significance has been performed.

3. Upstream seeding and the Northern Hemisphere storm tracks

a. Upstream seeding and the Pacific storm track

We first explore the relationship between Pacific storm-track intensity and upstream seeding by comparing geopotential height variance at 300 hPa over Asia (35°–65°N, 70°–120°E, hereafter called the "upstream domain") to the same variance within the Pacific storm track (20°–65°N, 160°E–160°W, hereafter called the "downstream domain") for all cold-season (defined in this paper as October through April) months. The upstream and downstream domains, together with a random sample of 100 disturbances that propagate through the upstream domain (out of a total of 3352 analyzed for all 301 months in this study), are shown in Fig. 1. The

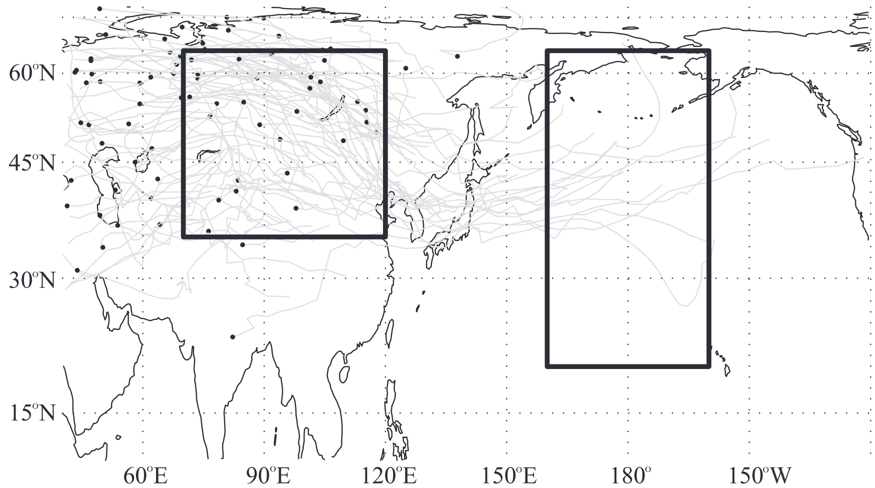

FIG. 1. Sample of 100 cyclonic disturbances that propagate through the upstream domain. Black dots represent cyclogenesis location, and gray lines represent the path of disturbance center. The upstream and downstream domains are indicated. Note that this sample represents , 0.1% of the 3352 upstream disturbances that are included in all analyses.

upstream domain's bounds are chosen because previous work (e.g., Wallace et al. 1988; Hakim 2003; Chang 2005) has shown that midlatitude Asia is the dominant source of seed disturbances for the Pacific storm track. The downstream domain's bounds are chosen to cover a large portion of the Pacific storm track, and also to be several Rossby radii downstream of the upstream domain. Results are insensitive to modest changes (i.e., ; 108–208 in any direction) to the location and sizes of these two domains.

A scatterplot comparing 300-hPa storminess in the upstream and downstream domains is shown in Fig. 2a, where storminess is defined as the bandpassed variance in geopotential height (see section 2). Every symbol represents the monthly average storminess for each of the seven cold season months and for 43 years between October 1958 and April 2001. Very similar results are obtained for meridional wind variance and for feature-tracking statistics at the same level (not shown, but discussed more in section 3c).

The first impression from Fig. 2a is that there is a great deal of scatter. This emphasizes that there is a large amount of seasonal and interannual variability in storminess, and mean climate phenomena emerge from this variability. However, it is also visually obvious, and perhaps not surprising given the geographic proximity of the two regions, that there is a positive correlation between the upstream and downstream domains. For all months together, the correlation coefficient of the data shown in Fig. 2a is 0.41, which is highly statistically significant (. 99%, see Table 1), and implies that about 17% of the observed variability in Pacific storm-track intensity is accompanied by variations in upstream storminess. While 17% may seem like a small fraction of the variance, it should be noted that this is comparable to other notable and meaningful fluctuations in storm-track intensity. For example, the MWM is manifest as a 25% reduction in the intensity of the Pacific storm track in the heart of winter (Julian days 10–25) compared to fall and spring (Julian days 300–325 and 90–115) (PRB10; also see Nakamura 1992), and comparing extreme strong and weak jet months in DJF, we find a 25% reduction in storminess in the downstream domain (this is the subject of section 4; also see Chang 2001).

Figure 2a also demonstrates the role of seeding and is consistent with the results of PRB10: midwinter months (filled black symbols) are clustered in the lower left of Fig. 2a (i.e., weak upstream seeding corresponds to weak storm-track intensity), whereas the transition seasons (open gray symbols) are not. On average, in winter (DJF) upstream seeding is 13% weaker, and the Pacific storm track is 8% weaker, than in the transition months (see also Table 2); for the 30-day window spanning the climatological MWM, upstream seeding is 60% weaker and the Pacific storm track is 25% weaker. Though the correlation shown here certainly does not demonstrate causality, it is consistent with the conclusion reached by PRB10: the MWM occurs primarily because there is a wintertime reduction in seeding. For a much more thorough examination of the upstream seeding relationship for the MWM, the reader is directed to PRB10 and the subsequent discussions in Chang and Guo (2011), Penny et al. (2011), and Chang and Guo (2012), as well as the discussion in section 3c of this paper.

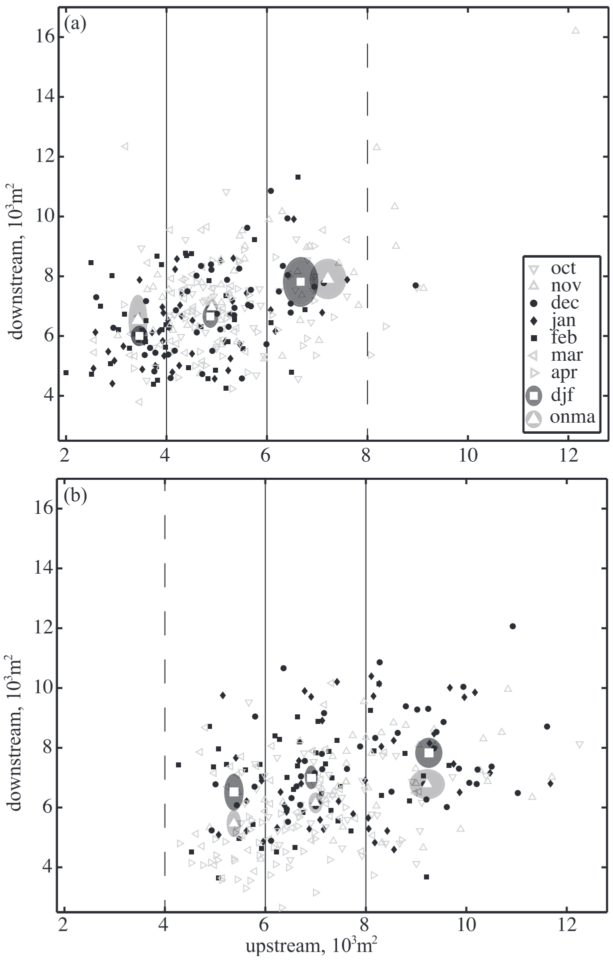

FIG. 2. Storminess ($\overline{Z'^2}$, 300 hPa) averaged in the upstream domain on the *x* axis compared to the downstream domain on the *y* axis for the seven cold season months between October 1958 and April 2001 within the (a) Pacific storm track and (b) Atlantic storm track. In addition to the raw monthly data (see key), both plots show means for weak, medium, strong, and very strong seeding cases for winter months (December/January/February, white squares, dark gray shaded ellipses for 95% confidence) and transition months (October/November/March/April, white triangles, light gray shaded ellipses for 95% confidence). Confidence intervals for the estimate of the mean are determined with a *t* test. For this and all subsequent figures, ''cold season'' months are October–April, ''winter'' months are DJF, and ''transition'' months are ONMA. For the ellipses in Fig. 2a, we consider the ''high'' and ''very high'' seeding regimes together for the Pacific.

The relationship between upstream and downstream storminess persists throughout the cold season. For all months the correlation is 0.41; for only the transition-season months [October, November, March, and April (ONMA)] it is 0.38; and for winter months (December, January, and February), it is 0.39 (Table 1). These correlations are statistically indistinguishable from each other. In this paper we focus on seasonal data because we want to maximize the amount of available data, but we have also considered year-to-year changes in a set calendar month. The correlation between upstream and downstream variance in six of the seven cold season months is statistically indistinguishable from that using all seven months (0.41, see Tables 1 and 3). The odd month out is April (correlation coefficient is 0.07). The weak relationship in April is consistent with results from PRB10, where a curious and notable spike in growth rates over the Pacific storm track in late spring was found.

TABLE 1. Correlation between monthly averaged storminess ($\overline{Z'^2}$, 300 hPa) in the upstream and downstream domains for the Pacific and Atlantic storm tracks. Bold indicates a correlation that is different from zero with 99% confidence (determined by a *t* test).

	Pacific	Atlantic
Oct–Apr	**0.41**	**0.37**
Dec–Feb	**0.39**	**0.30**
Oct, Nov, Mar, and Apr	**0.38**	**0.39**

b. Comparisons between the two Northern Hemisphere storm tracks

Although the primary focus of this paper is the North Pacific storm track, it is instructive to compare results with the North Atlantic storm track. Figure 2b was obtained for the variations in the Atlantic storm track at 300 hPa following the same methods that were used to obtain Fig. 2a for the Pacific storm track, with the exception that the upstream (358–658N, 1308W–1808) and downstream (208–658N, 408W–08) domains have been shifted 1608 to the east. For all months the correlation over the Atlantic is 0.37; for only the transition-season months (ONMA), it is 0.39; and for winter months (DJF), it is 0.30 (Table 1). Collectively these data indicate that, like the Pacific, the relationship between upstream seeding and downstream storminess persists throughout the cold season. Although it is not a difference that is statistically significant at 95%, the slight drop in correlation for the winter months relative to the transition seasons is a suggestion that seeding may be a less important control for Atlantic storminess in the depths of winter, when local conditions are exceptionally favorable for storm growth.

While the general characteristics of Fig. 2 for the Pacific and Atlantic are strikingly similar, there are some

TABLE 2. Fractional difference between storminess ($\overline{Z'^2}$) in Dec/Jan/Feb relative to Oct/Nov/Mar/Apr. Bold indicates that DJF and ONMA storminess are different with 95% confidence (determined by a *t* test for the difference between means).

	Pacific	Atlantic
Upstream domain	2 **13**%	1 3%
Downstream domain	2 **8**%	1 **15**%

TABLE 3. Individual monthly correlations between storminess ($\overline{Z'^2}$) in the upstream and downstream regions. Bold indicates a correlation that is different from zero with 95% confidence (determined by a t test). With the exception of April, each individual month is indistinguishible from the 7-month mean of 0.41. The correlation for ''All months'' is significant at the 99% level.

	Correlation
Oct	0.16
Nov	**0.63**
Dec	**0.45**
Jan	**0.44**
Feb	0.21
Mar	0.27
Apr	0.07
All months	**0.41**

important differences. For example, for the Atlantic, upstream seeding and downstream storminess are both strongest during winter: on average, in DJF upstream seeding is 3% stronger (an insignificant difference), and the Atlantic storm track is 15% stronger (a significant difference), than in ONMA (Table 2).

Furthermore, the Atlantic storm track is almost always more strongly seeded than the Pacific. For example, average upstream seeding is 58% higher in the Atlantic than the Pacific for the cold season average, and the biggest differences occur in winter (for DJF, average seeding is 70% higher in the Atlantic than in the Pacific). This may have some bearing on the observation that the Atlantic storm track is characterized by both less overall baroclinicity and also a 10%–15% stronger storm track than the Pacific (e.g., Kageyama et al. 1999; we have also calculated this in our dataset.). Our results raise the possibility that there is not a local or a nonlinear cause for this observation. Instead, it may simply be due to the fact that the Atlantic storm track is more strongly seeded than the Pacific. More work is needed to evaluate this suggestion.

When the Atlantic and Pacific are considered together, it is clear that the importance of upstream seeding is robust in both basins and for a wide range (fall through spring, Atlantic and Pacific) of background states. The data for both basins are next divided into four regimes based on the strength of the upstream seeding: weak (, 4000 m^2), medium (4000–6000 m^2), strong (6000–8000 m^2), and very strong (. 8000 m^2). In Fig. 2, the ellipses show the average of the data, partitioned into the different seeding regimes; a square in the center of an ellipse indicates the average of the weak, medium, strong, and very strong cases for winter (DJF) months, and a triangle surrounded by an ellipse indicates the average for the transition seasons (ONMA).

This division again underscores the fact that the Atlantic storm track is more strongly seeded than the Pacific. For example, in the Atlantic no months fall into the ''low'' seeding regime, while 81 months fall into the ''very high'' regime. In the Pacific, 70 months fall into the low seeding regime, and only 7 months fall into the very high regime. This division is robust to other choices of low and high seeding regimes. For example results are the same if we divide the data so that an equal number of months fall into low, medium, and high seeding regimes.

This division by the strength of the upstream seeding also provides insight into variations in Pacific and Atlantic storm-track intensity that occur independent of variations in upstream seeding. In each of its three seeding regimes (i.e., medium, strong, and very strong), the Atlantic storm track is significantly stronger in winter than it is during fall and spring. This is consistent with expectations from the simplest linear theories that a stronger jet causes increased baroclinicity, which results in increased local storminess. However, in each of the Pacific storm track's three seeding regimes (i.e., weak, medium, and strong), the mean storminess during winter months is not significantly different from the transition-season months despite the increase in baroclinicity in winter compared to the shoulder seasons.

The observation in the previous paragraph—that the wintertime Pacific storm track is essentially the same strength as the shoulder season storm track when the effects due to seeding are removed—helps shed light on seeming discrepancies and ongoing discussion in the literature concerning interannual, interseasaonal, and intraseasonal variations of the Pacific storm track. In particular, in the introduction we summarized several previous studies (e.g., Chang 2001; Zhang 1997; Christoph et al. 1997; Nakamura and Sampe 2002; Deng and Mak 2005) that found evidence that nonlinear processes (e.g., fast advection through the baroclinic zone, diabatic effects, and tropical teleconnections) inhibit the development of baroclinic waves within the wintertime Pacific storm track, and this led to a presumption that the MWM is caused by these nonlinear processes. PRB10 also found that the relationship between observed storminess and growth rates do not follow Eady model predictions, but their results show that upstream seeding (a linear process) is the dominant cause of the MWM. Chang and Guo (2011) and Chang and Guo (2012) questioned whether upstream seeding is indeed important for the MWM, but there are strong limitations to their analysis that we discuss in section 3c. The results presented here add further support to the interpretation that reduced upstream seeding is the dominant cause of the MWM, but they also show that other processes are clearly present and contribute. Further, our results underscore that the influence of the upstream wave source is limited; measurable effects should only be expected when there is a very strong signal from upstream, as there is for the MWM.

c. *Comparisons with recent work regarding the importance of upstream seeding for the Pacific storm track*

Results from a recently published paper are in apparent conflict with our results, and in this subsection we describe these discrepancies and defend the parameters chosen and conclusions drawn in this study. Chang and Guo (2012, hereafter CG12) analyzed the relationship between upstream seeding and downstream storminess for the North Pacific storm track and found that they are largely uncorrelated. We have found that the reasons for this discrepancy are due to the following: 1) different months considered (October through April in this study versus October, January, February, and April in CG12), 2) a difference in perspective as to whether cold season months are best viewed as one large dataset (this study) or individually (CG12), 3) different plotting and analysis conventions (retaining monthly means in this study versus monthly means removed in CG12), and 4) differences in field considered (Z variance in this study versus V variance in CG12). We address each of these reasons below in the order listed. After a careful analysis, we believe that while CG12 does present some interesting points that deserve further attention, their results are focused narrowly on only one aspect of Pacific storm-track variability—the MWM—and this limited scope causes CG12 to miss the overall relationship that exists between the two NH storm tracks and their upstream wave source. For those who are not concerned with this apparent conflict, we note that the reader can skip to section 4 with no loss in continuity.

1) In Fig. 2a, we divided the data into seeding regimes and showed that fall, winter, and spring have more or less the same strength Pacific storm track for each seeding regime. CG12 also divided the data into seeding regimes for the Pacific storm track, and found that fall and spring have a stronger Pacific storm track compared to winter (see their Fig. 1d). This discrepancy is almost entirely because CG12 considered only November, January, February, and April, whereas this study includes all seven cold season months between October and April. When we limit our analysis to include the same four months as CG12, we reproduce their result.

   Which choice is correct? Our primary goal in this section is to answer the following question: in the observational record, how important is upstream seeding for a downstream storm track? We chose to evaluate all seven cold season months to maximize the available data and to minimize noise. We feel strongly that including all of the available data is the better choice. CG12 includes only four months because the primary goal of that study is to address whether upstream seeding is responsible for the MWM. To avoid the artifact of calendar months altogether, PRB10 uses a 30-day running mean and finds that wintertime storminess is reduced by 25% relative to fall and spring, compared to the 15% reduction for January/February compared to November/April in CG12. However, this is not the focus of the present paper.

   An unfortunate consequence of CG12's choice of months is that the month of April weighs heavily in their analysis. As mentioned earlier, the upstream/downstream correlation in April, only 0.07, is the weakest of all seven months. Consistent with this weak correlation, previous work has shown that there is a notable maximum in cyclone growth rates during the month of April; feature-tracking calculations show that Pacific storm-track-averaged growth rates in April are higher than any other month (PRB10, their Fig. 7). This is consistent with the notable lack of importance of upstream seeding that both CG12 and this study observe for the month of April, and indicates that *April is the odd month out* for the seeding relationship in the Pacific storm track.

2) A fundamental difference between this study and CG12 is a difference of perspective. In this study we consider all seven cold season months together, without subtracting out a background state mean value for each month, and we feel strongly that there is value gained from this viewpoint. We justify our convention in several ways. First, as previously mentioned, the correlation between upstream and downstream variance in six of the seven cold season months is indistinguishable from that using all seven months. Second, in the multimonth dataset there is no evidence of a different seeding relationship for the individual months. For example, the slope of a best-fit line through all 301 points for the cold season Pacific storm track is 0.47 [95% confidence: ($-$0.02, 1.24), this is the solid black line in Fig. 3]. This is statistically indistinguishable from the seeding relationship using the monthly averaged data (seven points, the cyan solid line), or the category (weak, medium, and strong, three points for each season) averaged data (three points) for the winter and transition seasons. These relationships are shown in Fig. 3. Combined, the best-fit line through all 11 points (the

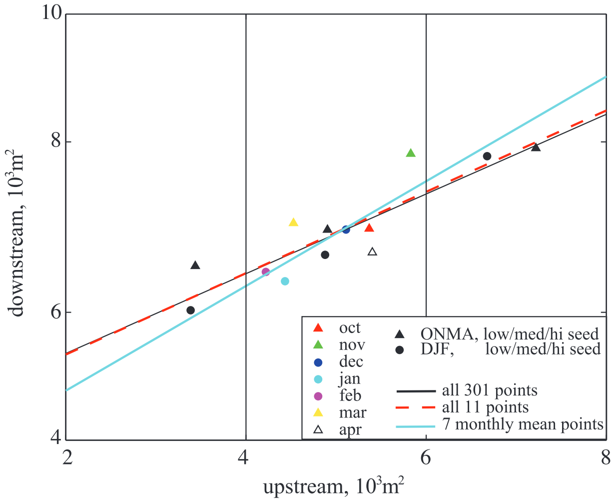

FIG. 3. Simplification of the data presented in Fig. 2a. The mean value each of the seven cold season months (October–April) are indicated by colors, and the mean value for DJF (circles) and ONMA (triangles) divided into low, medium, and high seeding regimes are in black. Best-fit linear regression lines are also indicated: the blue solid line is for the six cold season months, the red dashed line is for all 11 data points in this figure, and the black line is for all 301 points in Fig. 2a. As stated in the text, all three linear regression lines have a statistically identical slope to within 95% confidence.

seven months October–April plus the six averages for binning by the strength of the seeding and the season) in Fig. 3 has a slope of 0.48 [95% confidence: (0.32, 0.64), the dashed red line]—almost exactly the same as the slope (0.47) that we quoted above for best-fit line through all 301 data points. Third, in the multimonth dataset there is no evidence of spurious correlations; for example, each month has notable overlap along both the domain and range of Fig. 2.

3) While we feel the foregoing arguments are compelling, we recognize that this does not prove that all seven months are best viewed together as one collective dataset, and there are other ways to represent the data. CG12 represents the data by first removing a monthly mean from each data point before analyzing all data together, and they suggest that the significance we obtain is due to seasonality. This is not the case, however. With monthly means removed, the correlation coefficient between upstream seeding and downstream storminess drops from 0.41 to 0.36, a correlation that is statistically indistinguishable from that obtained when the monthly average is not subtracted from the data, and a correlation that is still positive with 99% confidence. Further, some drop in correlation is to be expected when monthly means are removed, because this removal does not reduce the scatter, but it does reduce the distance along the x and y axes that the data collectively span, and this results in a reduction in the ratio of signal to noise.

While we believe that CG12's technique to remove the monthly mean from each data point is unnecessary and perhaps even inappropriate, it is not unreasonable that some form of a background state should be removed. For example there is some suggestion that a background state should be removed in the results for the Atlantic storm track. Figure 2b for the Atlantic shows a separation in the strength of the winter (DJF) compared to the fall/spring (ONMA) storm track for the different seeding regimes, which suggests that processes local to the Atlantic storm track are also playing a role. Perhaps rather than removing monthly means (as in CG12) or nothing at all (this study), one should remove the difference relative to a linear trend, which is representative of all the data globally and is based on local baroclinicity. We refrain from performing this calculation because determining this linear trend would be highly subjective and would introduce a large uncertainty to the analysis. We have carefully considered the evidence and decided to present the results as we do in this paper because our analysis shows it to be an eminently reasonable way to represent the data.

4) The field chosen also provides an important contribution to the discrepancy (geopotential in this study versus meridional wind in CG12). When meridional wind variance is used to compute the correlation between upstream seeding and downstream storminess for the Pacific storm track, the correlation coefficient drops by 0.13, a barely significant difference,[1] and most of this drop is due to a drop in correlation during the winter months. We do not currently understand why this drop occurs, but it appears to be related to differences between two different measure of storminess, Z variance and V variance, in the upstream region. For example, the correlation between Z variance upstream V variance downstream does not drop (it is 0.39 for the 7-month dataset). It is possible that, being a higher-order field, $\overline{V'^2}$ is noisier and behaves more erratically in the upstream region, where there is a substantial influence from orography. It is also possible that there is a discrepancy because we have employed a 2–10-day temporal filter that

[1] Note that this drop is more notable than significance testing indicates, because geopotential and meridional wind are not independent from each other.

allows for longer time scales than the more common 2–6-day temporal filter. More work is needed to understand this discrepancy, but we have been unable to reach a resolution at this time. It is important to note that different measures of storminess often produce different results. In this instance the difference is enough to be important, but not to change the overall story: the 7-month correlation between upstream seeding and downstream storminess is always significant above 99%, and this is true independent of the choice of geopotential or meridional wind variance as well as whether the monthly means are removed.

Finally, there is another important difference in perspective between CG12 and this study. Our present study is focused on the relationship between seeding and storm-track intensity *throughout the cold season*, and for both of the Northern Hemisphere storm tracks. The focus of the CG12 study is on the relationship between the MWM and seeding. For the question that CG12 considers, the methods used in PRB10 are more appropriate that those used in either CG12 or in the present study. PRB10 employs feature tracking, which yields results that demand a straightforward and unambiguous interpretation: reduced wintertime upstream seeding plays a dominant role in the MWM. Noisy scatterplots here and in CG12 are only helpful for identifying obvious discrepancies for the MWM, of which there are none.

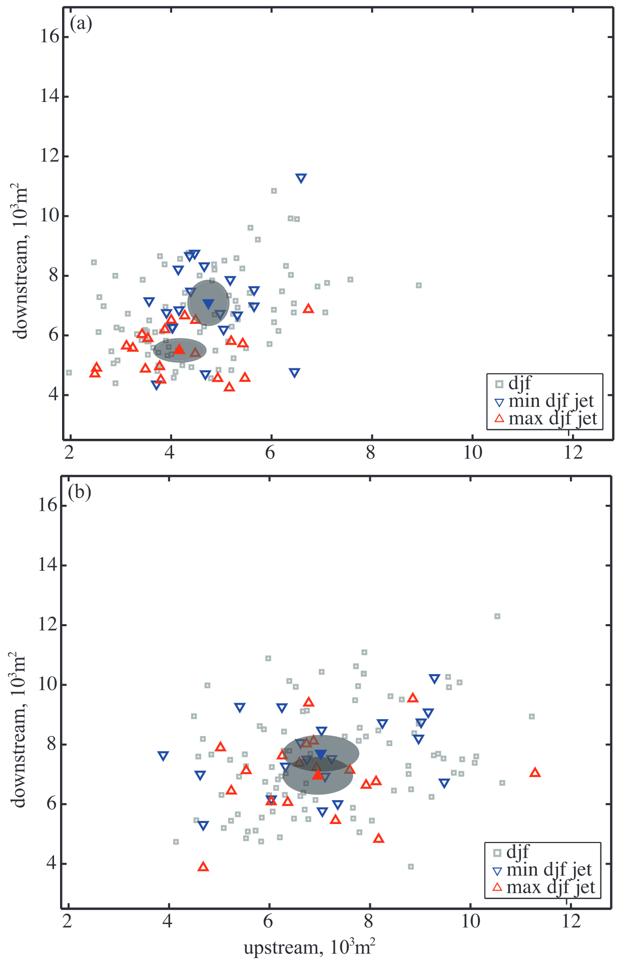

FIG. 4. As in Fig. 2, except for winter (DJF) months only in (a) the Pacific domain and (b) the Atlantic domain. Winter months with the top 20 jet-core strengths are indicated with a red upward-pointing triangle, the bottom 20 are indicated with a blue downward-pointing triangle, and all others are indicated with a gray square. Shaded ellipses indicate 95% confidence for the estimate of the mean (filled triangles) as determined from a *t* test.

4. The relationship between intraseasonal jet stream variability and the Pacific storm track in winter (DJF)

To this point, we have shown that upstream seeding exerts a robust and important control on downstream storm-track intensity for both the Pacific and Atlantic storm tracks. This relationship is maintained through tremendous changes in baroclinicity, bottom boundary condition, and atmospheric background state. In this section we begin by showing that, consistent with the results from others (e.g., Nakamura 1992; Chang 2001; Nakamura et al. 2002), over the Pacific there is a clear and counterintuitive inverse relationship between the wintertime jet stream variability and storm-track intensity. After establishing that this link in the intraseasonal wintertime variability does *not* occur because of seeding from the Asian continent, we examine both variance statistics and feature-tracking statistics to diagnose why it does occur.

Over the Pacific there is a clear relationship between jet strength and storminess that is additional to, and separate from, the upstream seeding relationship. In Fig. 4a the 20 winter (DJF) months with the strongest Pacific jet core are indicated in red (hereafter the "strong-core jet" months), the 20 winter months with the weakest Pacific jet core are indicated in blue (hereafter the "weak-core jet" months), and all other winter months (89 out of 129) are gray. We define the Pacific storm-track region as 25°–65°N, 160°E–160°W, which is the same as in section 3. For these results and all subsequent discussions, we define a metric of intraseasonal jet-core strength to be the wind speed at the core of the jet, calculated as maximum monthly averaged zonal wind speed within a 3D spatial grid that spans the entire North Pacific basin (20°–70°N, 120°E–220°W; 500–100 hPa) for the months of December, January, and February. We obtain almost identical results

Table 4. Comparison between feature-tracking statistics and Eulerian variance within the Pacific storm-track domain (20°–65°N, 160°E–160°W). Relative change is the average value during the strong-core jet months divided by the average value during the weak-core jet months. Here R, which is defined by Eq. (2) and explained in the text, is the relative change in Eulerian variance that is predicted by the feature-tracking statistics, and $\overline{Z'^2}$ is the observed relative change in Eulerian variance in the same location. All results are calculated at 300 hPa. Bold indicates that the strong-core jet months are different from the weak-core jet months with 95% confidence.

Relative change	$\overline{(Z')^2}$	No.	Amplitude	Wavelength	Velocity	R
Overall	**0.75**	0.99	**0.91**	**0.94**	**1.05**	**0.73**
Cyclonic	—	0.97	**0.92**	**0.94**	**1.04**	**0.73**
Anticyclonic	—	1.03	**0.89**	**0.94**	**1.05**	**0.74**

for other reasonable choices. For example, results are essentially the same if we consider 2-month averages, 3-month averages, or 1-month averages as shown here; if we consider only a spatial 2D grid near the jet stream level instead of a 3D grid that spans many vertical layers; or if we define winter as December/January/February, January/February, or January alone.

A relationship between jet-core strength and Pacific storm-track intensity is visually evident in Fig. 4a: when the wintertime Pacific jet core is strong (red triangles), the wintertime Pacific storm track is weak. On average, variance is 25% weaker in the strong-core months compared to the weak-core months, a highly significant difference (Table 4, hereafter we refer to this as the "inverse relationship" that occurs on intraseasonal time scales within the winter season). On the other hand, upstream seeding and jet-core strength appear to vary independently for the Pacific basin; for example, the correlation coefficient between monthly averaged jet-core strength and monthly averaged seeding is only −0.08 (not shown). There is some indication from Fig. 4 that months with a strong-core jet also have weaker upstream seeding, but this difference is not statistically significant and it is not robust to other choices of seasonality (e.g., if we only include January/February instead of December/January/February, then there is no relationship). Thus, we treat any cross correlations, such as the possibility that variability in seeding controls variability in the jet, as second-order effects that we do not consider.

For comparison, the equivalent plot for the Atlantic domain is also shown in Fig. 4b. Note that there is a hint of the same behavior for the Atlantic storm track, though it is not significant at 95%: when the Atlantic jet is strong, the Atlantic storm track is weak.

This inverse relationship that exists between jet-core strength and storminess on the intraseasonal time scale for the wintertime Pacific storm track has been documented and examined by several others (e.g., Chang 2001; Nakamura et al. 2002; Nakamura and Sampe 2002; Harnik and Chang 2004). Proposed explanations for the inverse relationship are quite diverse, spanning both linear and nonlinear dynamical mechanisms. In this section we use new results from both feature-tracking statistics and variance statistics to understand why there is an inverse relationship and to further evaluate previously proposed mechanisms.

a. Variance statistics

The inverse relationship between jet strength and Pacific storminess is first examined by comparing climatologies of months with a strong-core jet to those with a weak-core jet. A composite map of the jet stream

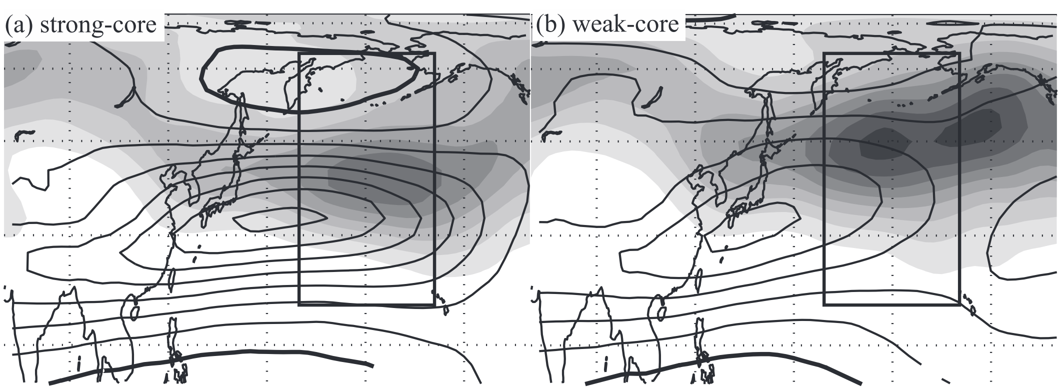

Fig. 5. Zonal winds (contours every 10 m s^{-1}, zero contour thick) and storminess ($\overline{Z'^2}$, shading every 1500 m^2 above 2000 m^2) at 300 hPa for the 20 (a) strong-core jet stream and (b) weak-core jet stream months. A box corresponding to the Pacific storm-track domain (20°–65°N, 160°E–160°W) is also indicated. Latitude lines are every 15°, and longitude lines are every 30°.

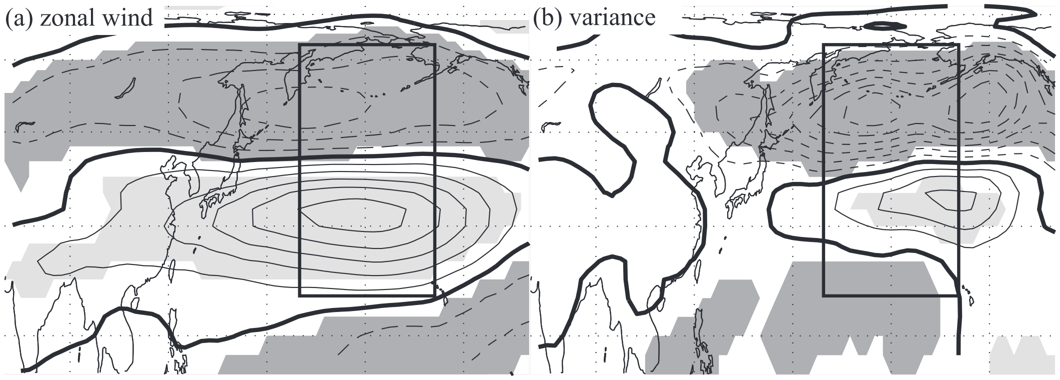

FIG. 6. Difference between (a) zonal wind strength, contours every 5 m s^{-1}, and (b) storminess ($\overline{Z'^2}$), contours every 1000 m^2. Both plots are strong-core jet months minus weak-core jet months, thick black contour for zero, solid for positive, dashed for negative, and shading where values are different from zero with 95% confidence (dark gray for negative, light gray for positive, determined from a *t* test). A box corresponding to the Pacific storm-track domain (20°–65°N, 160°E–160°W) is also indicated. Latitude lines are every 15°, and longitude lines are every 30°.

(zonal wind speed at 300 hPa, contours) and storm-track intensity (variance of 2–10-day-filtered geopotential height, $\overline{Z'^2}$ at 300 hPa, shading) for the strong-core jet months is shown in Fig. 5a, and weak-core jet months is shown in Fig. 5b.

As previously noted, the differences in jet stream structure between strong-core and weak-core months are much more extensive than just their maximum speed. The strong-core jet stream is meridionally narrow and zonally elongated. The weak-core jet stream is meridionally wide and tilts from southwest–northeast, a pattern that is more typical of a classic eddy-driven jet (e.g., Orlanski 1998). Remarkably, one of the only things that the two jet stream patterns share is their latitude of maximum wind speed: throughout almost the entire Pacific domain (90°–212.5°E), the latitude of maximum wind speed is the same for the strong-core and weak-core jets to within one 2.5° grid box. This lack of variability in jet location is robust; it is present when all winter months are considered, not just when only the strong and weak jet stream months are considered, and it supports the idea that there are strong external controls on the latitude of the Pacific jet stream (e.g., Lee and Kim 2003) from either tropical convection or the topographically controlled planetary stationary wave pattern.

Further comparison is made from the difference maps shown in Fig. 6. Figure 6a shows the difference in zonal wind strength between the strong-core jet and weak-core jet streams, and Fig. 6b shows the difference in variance, $\overline{Z'^2}$. In both of these maps, solid lines denote positive values (i.e., strong core greater than weak core), dashed lines denote negative values, light gray shading indicates values that are positive and different from zero with 95% confidence, and dark shading values that are negative and different from zero with 95% confidence. As is expected from the discussion in the previous subsection, upstream of the storm track there is very little difference in storminess between the strong-core and weak-core months, supporting our conclusion that upstream seeding is likely not playing an important role for the inverse relationship.

The most striking result from Fig. 6b, which has not been emphasized in previous studies, is that storminess is not reduced throughout the entire Pacific domain. In fact, there is a notable similarity between the two panels in Fig. 6: regions of enhanced storminess tend to be collocated with regions of strong jet stream winds, and vice versa for weak jet stream winds. Note that while the strong jet is over 25 m s^{-1} stronger than the weak jet at its core, the strong-core jet is so meridionally narrow that the westerly flow is as much as 15 m s^{-1} *weaker* in the midlatitudes between about 40° and 65°N. The inverse relationship that occurs in winter between jet-core strength and Pacific basin-average storminess occurs because the negative values in Fig. 6b are larger in both areal extent and amplitude than the positive values. From the above observations, we suggest that it is misleading to characterize the inverse relationship between jet-core strength and basin-average storminess as a striking anticorrelation throughout the Pacific.

b. Feature-tracking statistics

The relationship between jet stream structure and storminess is further illuminated using feature tracking. We begin by examining the number density and average amplitude of cyclonic disturbances, shown in Fig. 7 for the strong-core (Fig. 7a) and the weak-core (Fig. 7b) jet months.

The basic relationship between jet strength, number density, and disturbance amplitude is familiar and

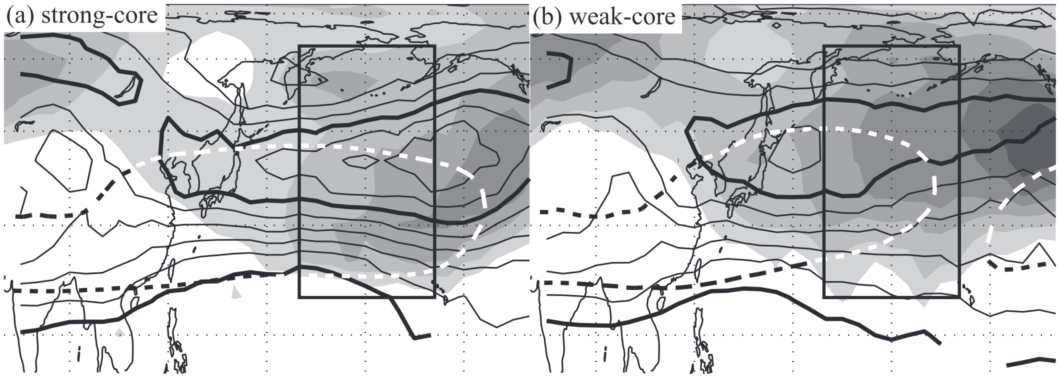

FIG. 7. Number density (contours every 1 disturbance per month per 10^{7} km$^{2\,2}$, bolded contours are 1 and 6 disturbances per month) and feature amplitude (shading, interval every 2 over 14 dm) in DJF for (a) the strong-core jet and (b) the weak-core jet months. The 30 m s$^{2\,1}$ zonal wind contour is indicated as a dashed white/black line for reference. A box corresponding to the Pacific storm-track domain (208–658N, 1608E–1608W) is also indicated. Latitude lines are every 158, and longitude lines are every 308.

robust. For example, in both strong-core and weak-core jet months, disturbance amplitude maximizes downstream and slightly equatorward of the maximum in number density, and number density is displaced slightly poleward from the core of the jet stream, with a maximum near the poleward flank of the jet exit region. In this section we show results for cyclonic disturbances only, but also discuss results for both cyclonic and anticyclonic disturbances where relevant. Somewhat surprisingly, the maps for cyclonic disturbances are qualitatively very similar to the corresponding maps for anticyclonic disturbances.

The spatial pattern of number density shows substantial differences between the strong-core and weak-core jet composites (Fig. 8a). In the strong-core months, there are more tracks in the core of the jet stream and fewer to the north and south, consistent with a narrower, more focused jet. A similar pattern is evident from the locations of cyclogenesis (not shown); in the strong-core jet months, there is very little cyclogenesis outside about 308–408N, whereas in the weak-core jet months, there is widespread genesis at all latitudes between 258 and 558N. Although it is visually striking, this difference in the pattern of number density does not account for the inverse relationship. Averaged over the Pacific domain (208–658N, 1608E–1608W), number density is only about 1% less in the months with a strong-core jet (3% less for cyclones and 3% more for anticyclones, see Table 4), a fraction that is not statistically significant. As anticipated from Figs. 7 and 8b, the primary reason that variance is

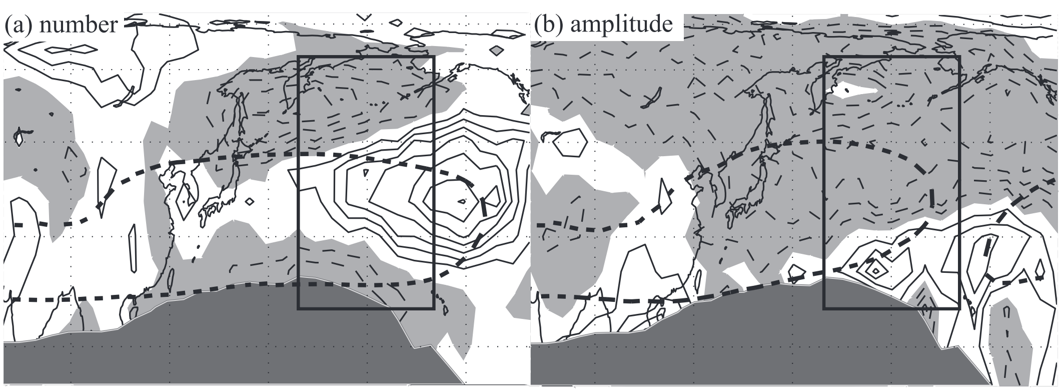

FIG. 8. Difference between (a) number density, contours every 0.5 disturbances per month per 10^{7} km$^{2\,2}$ and (b) feature amplitude, contours every 1 dm. Both plots are strong-core jet months minus weak-core jet months (dashed lines with gray shading for negative, solid lines with no shading for positive). Regions with less than 1 disturbance per month on average in either the strong-core or weak-core jet months are blocked from view. The 30 m s$^{2\,1}$ zonal wind contour is indicated as a dashed black line for reference. A box corresponding to the Pacific storm-track domain (208–658N, 1608E–1608W) is also indicated. Latitude lines are every 158, and longitude lines are every 308.

reduced in the strong-core months is because the amplitude of the storms is reduced.

One main advantage of feature-tracking statics is the ability to consider all aspects of storminess (disturbance speed, area, number, genesis, amplitude, growth rate, etc.) individually. While this division is extremely powerful, it can be difficult to place all of the numbers in context. PRB10 provided a framework to make a rough comparison between feature-tracking results and variance statistics through the simple analogy of a traveling wave pulse. In this framework, one can show that Eulerian variance is proportional to feature tracking through the relationship:

$$\overline{Z'^2} \propto N Z_0^2 \lambda c^{-1}, \quad (1)$$

where N is the number of disturbances, Z_0 is disturbance central amplitude, λ is disturbance wavelength, and c is disturbance speed. See PRB10's appendix B for a detailed formulation.

This scaling relationship allows for a direct comparison of Eulerian variance to a new metric that is based on feature-tracking statistics alone:

$$R \equiv \frac{\overline{Z'^2_{\text{strong jet}}}}{\overline{Z'^2_{\text{weak jet}}}} = \frac{(N Z_0^2 \lambda c^{-1})_{\text{strong jet}}}{(N Z_0^2 \lambda c^{-1})_{\text{weak jet}}}. \quad (2)$$

Eulerian variance is compared to feature-tracking results in Table 4 for all disturbances and for cyclonic and anticyclonic disturbances individually. Wavelength is interpreted as the characteristic length scale, and approximated as the square root of the area of the disturbance.[2] This new feature-tracking-based metric predicts that overall storminess should be reduced by 27% in the strong-core compared to the weak-core jet months, and this compares very well with the 25% reduction in Eulerian variance in the same region (see Table 4).

It is now simple to back out the relative importance individual aspects of storms that give rise to the inverse relationship. It is clear that disturbance amplitude is the biggest contributor to the inverse relationship; this term alone provides a 17% (i.e., $1 - 0.91^2$, see Table 4) reduction in overall storminess. Disturbance wavelength (−6%) and velocity (−5%) are much less important, though both do contribute a statistically significant amount; the number of disturbances contributes a negligible amount. Note that while spatial growth rates (i.e., the growth rate of a disturbance scaled by the distance that it travels) do not appear explicitly in this formulation, they are indirectly included and depend on the combination of amplitude and velocity together.

We caution against an overly quantitative interpretation of the results based on Eq. (2); while this calculation is valuable for a rough comparison, it greatly simplifies the relationship between Eulerian variance and feature-tracking statistics. The derivation assumes that storm tracks are composed entirely of a series of mobile, trackable, nonoverlapping, sine-shaped pulses.

We now use feature-tracking results to revisit some mechanisms that previous studies have suggested may be important to explain the inverse relationship. Previous studies have pointed out that rapid advection of eddies through the baroclinic zone when the jet is strong could play an important role in reducing the spatial growth rate of storms for both the MWS and the inverse relationship (e.g., Nakamura 1992; Nakamura et al. 2002). Our results show that disturbances travel about 5% faster in the strong-core relative to the weak-core months (Table 4), and this roughly corresponds to a 5% reduction in variance in the strong-core months relative to the weak-core months.[3] Rapid advection through the most baroclinic part of the Pacific storm track does not contribute much more; average disturbance speed in the baroclinic zone just upstream of the heart of the Pacific storm track (25°–40°N, 120°–160°E) is only about 6% faster in the strong-core months relative to the weak-core months. This result, which is included in Table 5, is consistent with previous work. Nakamura et al. (2002) computed a metric that is based on the Eady growth rate and the strength of mean-flow advection of eddies, and estimated that reduced eddy growth rate due to rapid advection through the baroclinic zone results in about a 5% reduction in storminess when the jet is strongest compared to when it is weakest.

Harnik and Chang (2004) presented an analytical analysis of the impact of a narrow, stronger jet on storminess, appealing to the ''barotropic governor'' effect (James 1987). They showed that eddy growth rate should be anticorrelated with jet-core strength when the jet stream is narrow, and suggested the effect may

[2] To calculate the average disturbance area, we first extract the filtered geopotential height field in a 20° × 20° region surrounding the center of each identified feature at each time step that each feature exists. Monthly average disturbance area is then estimated by compositing each extracted 20° × 20° region, counting the number of grid boxes in that region that are deeper than 100 m, and area weighting by $\sin^2$(lat).

[3] Note that disturbance speed is even less important for the MWM, counter to a suggestion in CG12. PRB10 calculated that the velocity of disturbances is only 3% faster in winter compared to the shoulder seasons. It is this difference in velocity that roughly accounts for the difference between a spatial and a temporal growth rate.

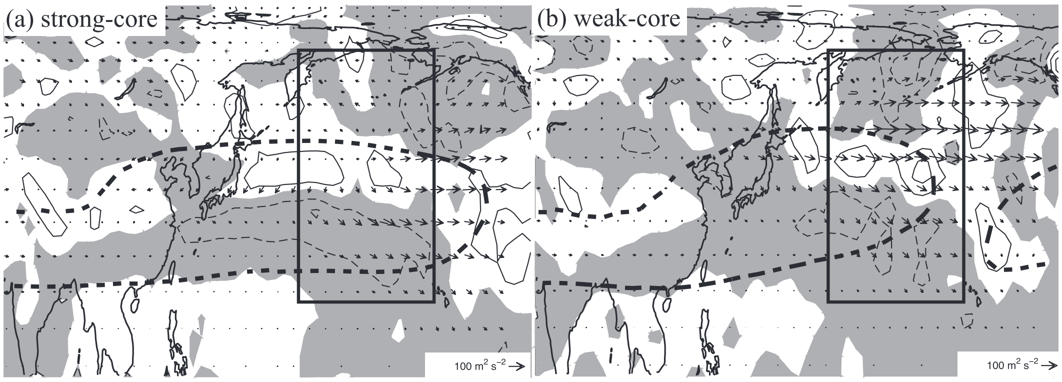

FIG. 9. Horizontal component of **E** vectors at 300 hPa (arrows) and divergence of **E** vectors at the same level (contours every 3 m s^{-1} day^{-1}) for the (a) strong-core and (b) weak-core jet months. Positive contours are solid lines with no shading, and negative contours are dashed lines with gray shading. The 30 m s^{-1} zonal wind contour is indicated as a dashed black line for reference. A box corresponding to the Pacific storm-track domain (20°–65°N, 160°E–160°W) is also indicated. **E**-vector arrows are plotted every 5°.

be strong enough to be relevant for the observed inverse relationship. To achieve analytical solutions, however, they had to assume that the wavelength of the eddies scales directly with the meridional width of the jet stream. For the Pacific jet, this turns out to be a poor assumption. We have analyzed the wavelength of disturbances in strong-core and weak-core months from the feature-tracking data, and found that the average wavelength of disturbances during strong-core jet months is only about 6% less than those in weak-core jet months. This is in the right direction to support Harnik and Chang (2004); however, the full-width, half maximum of the jet stream in the strong-core months is 42% less than that for the weak-core months.[4] Hence, it is not clear how the results from Harnik and Chang (2004) inform upon the real atmosphere for this case.

Overall, the feature-tracking statistics indicate that Pacific domain storms are less likely to become deep, mature disturbances in the strong-core jet months (see, e.g., Fig. 8a). During these months, disturbances are apparently unable to utilize locally available potential energy and this limits their growth and overall amplitude. Both of the previously proposed mechanisms that we can directly test (advection and the barotropic governor) can at most provide only a minor part of the explanation.

c. E vectors

To this point we have treated the jet stream as an independent forcing of the storm track, however, there are feedbacks between the two. To investigate these feedbacks, we calculate Eliasson–Palm flux vectors (**E**) in the 2–10-day filtered fields. Recall that the direction of **E** vectors corresponds to the direction of Rossby wave propagation, and that regions of **E**-vector divergence (positive contours) correspond to regions of momentum convergence from the transient eddies to the atmosphere's background state and will increase the zonal wind (and thus accelerate the jet, e.g., Edmon et al. 1980). The horizontal component, $E_H = (\overline{v'^2 - u'^2}, -\overline{u'v'})$ together with its divergence at 300 hPa, are shown in Fig. 9. The divergence field is, as expected for a spatial derivative, relatively noisy, but the individual maxima and minima are significantly different from zero, which adds confidence to our interpretation of the overall patterns.

In the weak-core months (Fig. 9b), the **E** vectors indicate that the primary role of transient eddies is to spread out and maintain a diffuse eddy-driven jet stream. West of about 170°W, in the midlatitudes (on the poleward flank of the jet), **E** vectors point nearly due east, and eddies act to reinforce the jet stream: there is strong eddy propagation and momentum convergence (i.e., white areas in Fig. 9b) in the core of the jet stream and divergence on both the poleward and equatorward flanks. Near the downstream end of the storm track, there is momentum convergence over a broad region that extends meridionally from the subtropics to the pole, and the most substantial region of convergence is near the Aleutian low. Overall, the weak-core months are reminiscent of a canonical picture Pacific storm-track

[4] PRB10 found that for the MWM the wavelength of winter disturbances is actually 7% *longer* in winter compared to fall and spring. Furthermore, as Harnik and Chang (2004) point out, the wintertime jet stream is only slightly narrower than the shoulder season jet stream. Hence, the narrowness of the climatological jet is unlikely to play a role in the MWM.

storms: eddies grow in the baroclinic zone off the Asian coast, propagate poleward over their lifetimes, and reach maturity and eventually decay near the Aleutian low (e.g., Thorncroft et al. 1993).

In the strong-core jet months (Fig. 9a), the **E** vectors indicate a very different picture. Here, eddies act to maintain a strong, narrow, elongated, and more subtropical jet stream across the entire Pacific domain. West of 170°W, in the midlatitudes, **E** vectors have a more southward orientation and the overall amplitude of eddy propagation is much weaker, compared to the weak-core jet months. Similar to the weak-core months there is momentum convergence in the core and divergence on the flanks of the jet stream. At the downstream end of the storm track, east of about 170°W, eddies act to zonally elongate and accelerate a narrower, more subtropical jet stream. For example, in the vicinity of the Aleutian low, there is momentum divergence (i.e., jet deceleration, gray shading in Fig. 9b), which is opposite from the weak-core months. In the strong-core jet months, there is a large region of momentum convergence on the subtropical flank of the jet stream off the coast of the Baja California where cutoff lows, large ridging events, and other atypical flow patterns, are common (e.g., Ndarana and Waugh 2010).

To summarize, in the strong- and weak-core months the transient eddies behave very differently, yet in both states the role of the transients is to reinforce the observed jet. This is consistent with previous work; simple modeling studies performed by Chang and Guo (2007) also found that eddies in the Pacific provide feedback to partially maintain the jet difference as qualitatively suggested by Fig. 9. However, from the results of Seager et al. (2003) and Chang and Guo (2007) it is also clear that on the seasonally averaged time scale, remote forcings (i.e., tropical diabatic heating and remote eddy forcing) are important for the difference between the strong- and weak-core jet streams. In addition, the **E** vectors indicate substantial structural and life cycle changes between transient eddies in the weak- and strong-core jet streams, with the archetypal picture of Pacific storminess in the former and a more atypical picture in the latter.

Finally, another striking feature is the presence of greater equivalent-barotropic flow in the strong-core relative to the weak-core jet streams (Fig. 10). Several classic modeling studies (e.g., Thorncroft et al. 1993; Hartmann and Zuercher 1998) found that the addition of barotropic flow causes the life cycles of baroclinic waves to transition sharply from anticyclonic (LC1 type) to cyclonic (LC2 type) behavior. There is some indication that there are more LC1-type disturbances in the weak-core jet; for example regions of momentum convergence are

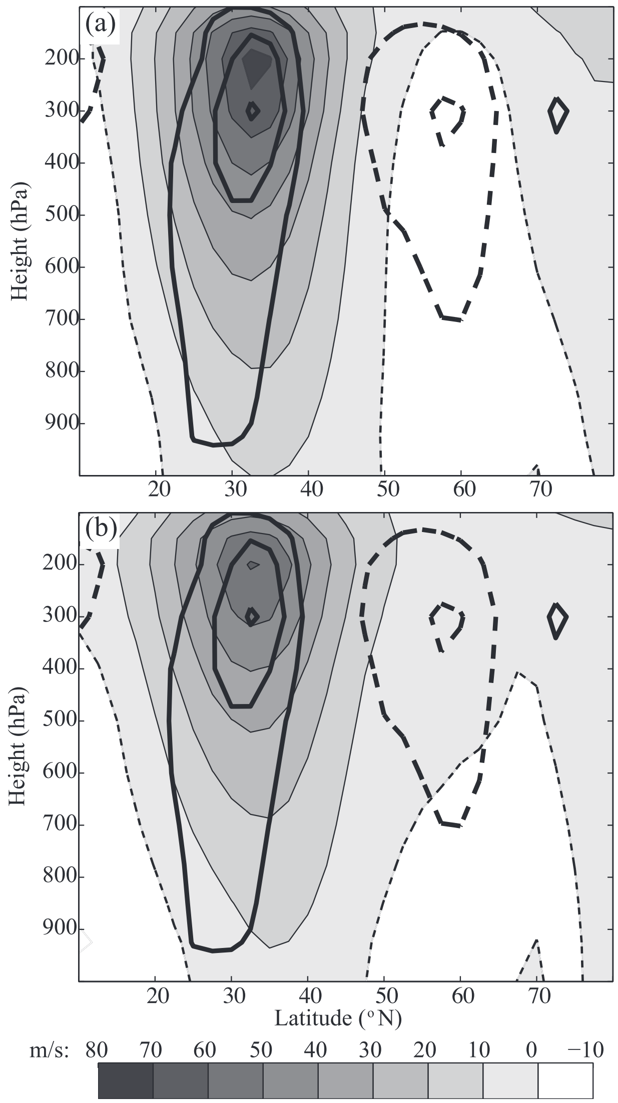

FIG. 10. Vertical structure of zonal winds at 180° for the (a) strong-core jet stream and (b) weak-core jet stream. Shading interval is every 10 m s^{-1}, zero contour is dashed. Difference between the two jet streams (strong minus weak) are indicated on both plots with contours every 5 m s^{-1}, zero line is omitted.

spread meridionally over a broad area in the eastern Pacific (see Table 5 and Fig. 9). However, LC1-type storms are traditionally viewed as smaller-amplitude, short-lived storms, which is opposite from what is observed. Thus, while these analyses certainly fall short of a quantitative demonstration, they point to a way forward for reconciling the literature on the inverse relationship with that on the life cycles of baroclinic waves.

5. Summary and conclusions

In this paper we have examined how variations in two mechanisms, upstream seeding and jet-core strength,

TABLE 5. Evaluation of previously proposed mechanisms for the inverse relationship. The first column lists mechanisms that have been proposed to explain why there is an inverse relationship. The second column is the importance of these mechanisms based on the results of this study. Note that these mechanisms are not all independent from each other, but they are included for completeness.

Mechanism	Likelihood
Reduced upstream seeding	Very unlikely
Fast advection through the baroclinic zone	Some effect; we estimate ; 5%
Narrower jet stream reduces linear growth rates (i.e., barotropic governor)	Unclear, but likely less than current linear modeling estimates
Barotropic shear causes transition to anticyclonic wave breaking	Possibly very important, but inconclusive in our results
Strong winter monsoonal flow	Not evaluated; not necessarily independent from other mechanisms
Wave trapping by strong subtropical jet	Not evaluated; not necessarily independent from other mechanisms
Diabatic effects	Not evaluated

relate to storminess within the cold season Pacific storm track. We found that the two mechanisms vary independently and we treat them as such.

In section 4, we examined how intraseasonal variations in the Pacific jet core during winter are related to Pacific storm-track intensity. To the picture that already exists in the literature, we add four main observations. First, the inverse relationship is not a striking anticorrelation when viewed spatially; regions with stronger-than-average jet stream winds tend to have stronger-than-average storminess, and likewise regions with weaker winds have weaker storminess; this is true for both the strong- and weak-core jet months. Second, upstream seeding does not explain why winter months with a strong Pacific jet core tend to be accompanied by weaker-than-average storm tracks. This is in contrast to the climatological MWM, where seeding plays a dominant role (PRB10). It has been common in the literature to treat these two phenomena as analogous, however, our results here and in PRB10 (and elsewhere; e.g., see Chang 2001) show that this is not appropriate. Third, we explore various proposed explanations for the inverse relationship (Tables 4 and 5). Excessive advection does not appear to be very important, accounting for , 5% reduction in variance in the strong-core jet months relative to the weak-core jet months. The barotropic governor effect is likely less than predicted by Harnik and Chang (2004), because our new observations of the wavelength of eddies show that eddy length scale does not scale directly with the width of the jet stream, but the exact effect remains to be determined. The predominant reason for the inverse relationship between storminess and jet-core strength is in the amplitude of storms: disturbances rarely become deep, mature systems when the jet core is strongest. In the strong-core jet months relative to the weak-core jet months there is not a shortage of storms; however, the amplitude of disturbances is significantly weaker (9%). Fourth, transient eddies act to reinforce the observed jet stream patterns for both the strong- and weak-core jet streams, and so the jet structure differences are consistent with the way that eddies are forcing the background flow. Pursuant to this last point, there are some indications that the strong- and weak-core jet streams are preferentially composed of LC2- and LC1-type storms, respectively, consistent with there being more barotropic shear in the strong-core jet months (Fig. 9), but more work is needed to evaluate this suggestion.

In section 3, we examined the climatological relationship between upstream seeding and downstream storminess, and found that about 17% of observed Pacific storminess covaries with upstream seeding (the exact percentage changes with modest modifications to the locations of the two domains or if we consider relative vorticity or meridional wind instead of geopotential height). This relationship persists through the entire cold season and in both the Atlantic and Pacific basins.

The analyses in section 3 add further support to the conclusion in PRB10 that the MWM occurs primarily because there is a notable lack of storminess upstream of the Pacific storm track in the heart of winter. However, nonlinear dynamics local to the Pacific storm track must be at least partially at play during the MWM: when variability due to upstream seeding is regressed out of the data (see the ellipses in Fig. 2a), we see that Pacific storm-track intensity is essentially constant throughout the cold season, despite greater baroclinicity in midwinter. As discussed at the end of section 3, these results help clarify some seeming discrepancies in the literature about the causes of both the MWM and the intraseasonal inverse relationship.

Last, the results presented here and in PRB10 lead us to consider a fundamental climate question: can upstream seeding be viewed as random chaotic noise? In most cases, we believe that the answer is likely "yes." We have shown that upstream seeding has a measurable and notable effect on downstream storminess, but the relationship is noisy (e.g., Fig. 2) and the results are somewhat dependent on the method used to measure storminess (CG12). Furthermore, the effect on storm-track intensity is approximately linear: the observations do not indicate a threshold behavior wherein seeding is a more effective forcing when it is particularly strong or particularly weak. However, we now have observational evidence that the answer to the posed question is ''no'' in some circumstances. In this paper, we noted that the Atlantic storm track is more strongly seeded than the Pacific storm track on average, and hypothesized that this may help explain why the Atlantic storm track is stronger overall than the Pacific. PRB10 found that a wintertime reduction in upstream seeding, which is related to a wintertime increase in static stability over Asia, is a dominant cause of the MWM. Donohoe and Battisti (2009) also found evidence that reduced seeding of the Atlantic during the Last Glacial Maximum, related to the presence of the Laurentide Ice Sheet over North America, resulted in a weak Atlantic storm track. These studies and others (e.g., Orlanski 2005; Zurita-Gotor and Chang 2005) have raised many questions about the role of seeding in controlling the strength of the major storm tracks. Aside from seeding's demonstrated impact on the MWM, the large amount of natural variability may be masking its other impacts, given the length of the observational record. Hence, long-term integrations of climate models are a possible next step.

Acknowledgments. We are grateful to four anonymous reviewers for their comments, which have greatly improved the text of this manuscript. This work was funded by National Science Foundation Continental Dynamics Grants 6312293 and EAR-0507431.

REFERENCES

Blackmon, M. L., 1976: Climatological spectral study of 500-mb geopotential height of the Northern Hemisphere. *J. Atmos. Sci.,* **33,** 1607–1623.

——, J. M. Wallace, N. C. Lau, and S. L. Mullen, 1977: Observational study of Northern Hemisphere wintertime circulation. *J. Atmos. Sci.,* **34,** 1040–1053.

Chang, E. K. M., 2001: GCM and observational diagnoses of the seasonal and interannual variations of the Pacific storm track during the cool season. *J. Atmos. Sci.,* **58,** 1784–1800.

——, 2005: The impact of wave packets propagating across Asia on Pacific cyclone development. *Mon. Wea. Rev.,* **133,** 1998–2015.

——, and Y. Guo, 2007: Dynamics of the stationary anomalies associated with the interannual variability of the midwinter Pacific storm track: The roles of tropical heating and remote eddy forcing. *J. Atmos. Sci.,* **64,** 2442–2461.

——, and ——, 2011: Comments on ''The source of the midwinter suppression in storminess over the North Pacific.'' *J. Climate,* **24,** 5187–5191.

——, and ——, 2012: Is Pacific storm-track activity correlated with the strength of upstream wave seeding? *J. Climate,* **25,** 5768–5776.

Charney, J., 1947: The dynamics of long waves in a baroclinic westerly current. *J. Meteor.,* **4,** 135–162.

Christoph, M., U. Ulbrich, and P. Speth, 1997: Midwinter suppression of Northern Hemisphere storm track activity in the real atmosphere and in GCM experiments. *J. Atmos. Sci.,* **54,** 1589–1599.

Deng, Y., and M. Mak, 2005: An idealized model study relevant to the dynamics of the midwinter minimum of the Pacific storm track. *J. Atmos. Sci.,* **62,** 1209–1225.

Donohoe, A., and D. S. Battisti, 2009: The amplitude asymmetry between synoptic cyclones and anticyclones: Implications for filtering methods in feature tracking. *Mon. Wea. Rev.,* **137,** 3874–3887.

Eady, E. T., 1949: Long waves and cyclone waves. *Tellus,* **1,** 33–42.

Edmon, H., B. Hoskins, and M. Mcintyre, 1980: Eliassen–Palm cross sections for the troposphere. *J. Atmos. Sci.,* **37,** 2600–2616.

Frederiksen, J. S., 1978: Instability of planetary waves and zonal flows in two-layer models on a sphere. *Quart. J. Roy. Meteor. Soc.,* **104,** 841–872.

——, 1979: Baroclinic instability of zonal flows and planetary waves in multi-level models on a sphere. *J. Atmos. Sci.,* **36,** 2320–2335.

——, and C. S. Frederiksen, 2007: Interdecadal changes in Southern Hemisphere winter storm track modes. *Tellus,* **59A,** 599–617.

Hakim, G., 2003: Developing wave packets in the North Pacific storm track. *Mon. Wea. Rev.,* **131,** 2824–2837.

Harnik, N., and E. K. M. Chang, 2004: The effects of variations in jet width on the growth of baroclinic waves: Implications for midwinter Pacific storm track variability. *J. Atmos. Sci.,* **61,** 23–40.

Hartmann, D., and P. Zuercher, 1998: Response of baroclinic life cycles to barotropic shear. *J. Atmos. Sci.,* **55,** 297–313.

Hodges, K. I., 1994: A general method for tracking analysis and its application to meteorological data. *Mon. Wea. Rev.,* **122,** 2573–2586.

——, 1995: Feature tracking on the unit sphere. *Mon. Wea. Rev.,* **123,** 3458–3465.

——, 1999: Adaptive constraints for feature tracking. *Mon. Wea. Rev.,* **127,** 1362–1373.

Hoskins, B. J., and K. I. Hodges, 2002: New perspectives on the Northern Hemisphere winter storm tracks. *J. Atmos. Sci.,* **59,** 1041–1061.

Ioannou, P., and R. Lindzen, 1986: Baroclinic instability in the presence of barotropic jets. *J. Atmos. Sci.,* **43,** 2999–3014.

James, I., 1987: Suppression of baroclinic instability in horizontally sheared flows. *J. Atmos. Sci.,* **44,** 3710–3720.

Kageyama, M., P. Valdes, G. Ramstein, C. Hewitt, and U. Wyputta, 1999: Northern Hemisphere storm tracks in present day and last glacial maximum climate simulations: A comparison of the European PMIP models. *J. Climate,* **12,** 742–760.

Lee, S., and H.-K. Kim, 2003: The dynamical relationship between subtropical and eddy-driven jets. *J. Atmos. Sci.,* **60,** 1490–1503.

Li, C., and D. S. Battisti, 2008: Reduced Atlantic storminess during last glacial maximum: Evidence from a coupled climate model. *J. Climate,* **21,** 3561–3579.

Lindzen, R. S., and B. Farrell, 1980: A simple approximate result for the maximum growth rate of baroclinic instabilities. *J. Atmos. Sci.,* **37,** 1648–1654.

Nakamura, H., 1992: Midwinter suppression of baroclinic wave activity in the Pacific. *J. Atmos. Sci.,* **49,** 1629–1642.

——, and T. Sampe, 2002: Trapping of synoptic-scale disturbances into the North-Pacific subtropical jet core in midwinter. *Geophys. Res. Lett.,* **29,** 8184, doi:10.1029/2002GL015535.

——, and A. Shimpo, 2004: Seasonal variations in the Southern Hemisphere storm tracks and jet streams as revealed in a reanalysis dataset. *J. Climate,* **17,** 1828–1844.

——, T. Izumi, and T. Sampe, 2002: Interannual and decadal modulations recently observed in the Pacific storm track activity and east Asian winter monsoon. *J. Climate,* **15,** 1855–1874.

Ndarana, T., and D. W. Waugh, 2010: The link between cut-off lows and Rossby wave breaking in the Southern Hemisphere. *Quart. J. Roy. Meteor. Soc.,* **136,** 869–885.

Orlanski, I., 1998: Poleward deflection of storm tracks. *J. Atmos. Sci.,* **55,** 2577–2602.

——, 2005: A new look at the Pacific storm track variability: Sensitivity to tropical SSTs and to upstream seeding. *J. Atmos. Sci.,* **62,** 1367–1390.

Park, H.-S., J. C. H. Chiang, and S.-W. Son, 2010: The role of the Central Asian Mountains on the midwinter suppression of North Pacific storminess. *J. Atmos. Sci.,* **67,** 3706–3720.

Penny, S., G. H. Roe, and D. Battisti, 2010: The source of the midwinter suppression in storminess over the North Pacific. *J. Climate,* **23,** 634–648.

——, ——, and ——, 2011: Reply. *J. Climate,* **24,** 5192–5194.

Seager, R., N. Harnik, and Y. Kushnir, 2003: Mechanisms of hemispherically symmetric climate variability. *J. Climate,* **16,** 2960–2978.

Thorncroft, C., B. Hoskins, and M. Mcintyre, 1993: Two paradigms of baroclinic-wave live-cycle behavior. *Quart. J. Roy. Meteor. Soc.,* **119,** 17–55.

Uppala, S. M., and Coauthors, 2005: The ERA-40 Re-Analysis. *Quart. J. Roy. Meteor. Soc.,* **131,** 2961–3012.

Wallace, J. M., G. H. Lim, and M. L. Blackmon, 1988: Relationship between cyclone tracks, anticyclone tracks, and baroclinic waveguides. *J. Atmos. Sci.,* **45,** 439–462.

Yin, J., 2002: The peculiar behavior of baroclinic waves during the midwinter suppression of the Pacific storm track. Ph.D. thesis, University of Washington, 137 pp.

Zhang, Y. Q., 1997: On the mechanisms of the mid-winter suppression of the Pacific storm track. Ph.D. thesis, Princeton University, 152 pp.

——, and I. M. Held, 1999: A linear stochastic model of a GCM's midlatitude storm tracks. *J. Atmos. Sci.,* **56,** 3416–3435.

Zurita-Gotor, P., and E. K. M. Chang, 2005: The impact of zonal propagation and seeding on the eddy-mean flow equilibrium of a zonally varying two-layer model. *J. Atmos. Sci.,* **62,** 2261–2273.